(NASA-CR-175809) ON THE USE OF A SUNWARD-LIBRATION-POINT ORBITING SPACECRAFT AS AN IMF MONITOR FOR MAGNETOSPHERIC STUDIES (Jet Propulsion Lab.) 25 p HC A02/MF A01 CSCL 04A G3/46

N85-27426

Unclas 21315

ON THE USE OF A SUNWARD-LIBRATION-POINT ORBITING SPACECRAFT AS AN IMF MONITOR FOR MAGNETOSPHERIC STUDIES

T. J. Kelly, N. U. Crooker, G. L. Siscoe

Department of Atmospheric Sciences, UCLA, Los Angeles, CA 90024

C. T. Russell

Institute of Geophysics and Planetary Physics, UCLA, Los Angeles, CA 90024

E. J. Smith

Jet Propulsion Laboratory, California Institute of Technology,

Pasadena, CA 91109

Abstract. Magnetospheric studies often require knowledge of the orientation of the IMF. In order to test the accuracy of using magnetometer data from a spacecraft orbiting the sunward libration point for this purpose, the angle between the IMF at ISEE 3, when it was positioned around the libration point, and at ISEE 1, orbiting Earth, has been calculated for a data set of two-hour periods covering four months. For each period, a ten-minute average of ISEE 1 data is compared with ten-minute averages of ISEE 3 data at successively lagged intervals. At the lag time equal to the time required for the solar wind to convect from ISEE 3 to ISEE 1, the median angle between the IMF orientation at the two spacecraft is 20°, and 80% of the cases have angles less than 36°. The results for the angles projected on the y-z plane are essentially the same. The minimum angle between the IMF orientation at the two spacecraft has a median of 11°, with 80% less than 19°. These low values indicate little temporal or small scale variation between the spacecraft. The minimum angle generally occurs at a lag time different from the convection time. The sign of the difference depends on IMF orientation in the sense that magnetic features tend to arrive sooner when the IMF is directed along the line between the spacecraft. However, the difference between a lag time appropriate to this corotation geometry and the convection lag time is not large enough to produce a significant decrease in the angles between the IMF vectors at the two spacecraft. We conclude that the IMF at a libration-point-orbiting spacecraft, lagged by the time required for the solar wind to convect to the earth, is a good, convenient predictor of the IMF near the earth.

Introduction

Knowledge of the orientation of the interplanetary magnetic field (IMF) just upstream of the earth is essential for studies of its interaction with the magnetosphere [e.g., Burch, 1983]. In the past, satellites in earth orbit could monitor the IMF only along the limited portions of their orbits which fell outside the bow shock. Continuous measurements of the IMF became available with the launch ISEE 3 in 1978 into a halo orbit around the libration point, ~230 R_E upstream. However, from this position the solar wind requires about one hour to convect downstream to the earth. Since the IMF is highly variable in time and space, it is important to test how accurately the ISEE 3 measurements can represent the IMF in earth's vicinity.

Two studies of the correlations between magnetometer measurements from ISEE 1 and ISEE 3 already have been performed. Russell et al. [1980] found that the degree of correlation often changes drastically in consecutive three-hour intervals, and Crooker et al. [1982] show that the degree of correlation increases with the variance of the IMF and decreases significantly for spacecraft separations perpendicular to the earth-sun line greater than 90 R_E. Also, King [1983] found relatively good correlations between hourly averages of measurements made by the earth-orbiting IMP 8 and ISEE 3 for a wide range of solar wind parameters.

The present study addresses more directly the question of how well the IMF orientation can be predicted near the earth from the upstream measurements. The angle between field orientations at ISEE 1 and ISEE 3 is calculated for two predicted lag times and compared to the minimum angle between the fields in the two-hour interval following the time of the ISEE 3 measurement. The minimum angle gives the limit on how well the IMF orientation

can be predicted at any given time. Histograms of these angles are then compiled from measurements covering a four-month period, and from them one can obtain the probability that the IMF orientation at the upstream libration point is within a certain angle of its orientation near the earth. Also statistical information is obtained on the accuracy of predicted time lags.

Data

Nearly continuous magnetometer data from ISEE 1 and ISEE 3 were obtained for the period from July 25 to Nov. 27, 1979. Times chosen for analyses were limited to intervals when the earth orbiting ISEE 1 was located upstream of the bow shock. The spatial coverage of the satellite orbits during this period are shown in Figure 1 in GSE coordinates. The orbit of ISEE 3 ranged from 195 to 265 R_E along the x axis and reached distances of approximately 100 R_E away from the x axis, in the y-z plane. The x distances correspond to solar wind transit times to earth on the order of one hour for typical solar wind speeds. The shaded region indicates coverage of the ISEE 1 orbit. It shows that the intersatellite separation distances in the y-z plane ranged from 18 to 105 R_E.

Measurements of solar wind velocity were required to calculate the solar wind transit times from ISEE 3 to ISEE 1. Ninety-minute averages of velocity were obtained from the Los Alamos solar wind experiment on ISEE 3 (supplied to data pool by S. J. Bame, principal investigator).

Analysis and Results

Time Variations of Angular Differences. The angle between the magnetic field orientations at ISEE 1 and ISEE 3 was calculated as a function of lag time for 885 two-hour data segments overlapped by one hour. A ten-minute average of ISEE 3 data was compared to successive ten-minute running averages of ISEE 1 data at one-minute intervals. Angles were calculated both between the total magnetic field vectors and between their projections in the y-z plane, perpendicular to the earth-sun line.

Averages over ten minutes were chosen because ten minutes is roughly the minimum length of time required for the magnetosphere to respond to changes in IMF orientation. Averages over 5, 20, and 60 min were tested; but the shorter time gave noisy results, and the longer times tended to mask the degree of agreement between the two field orientations.

Examples of the results are shown in Figure 2. Solar wind speeds ranged from 340 to 425 km/s during these intervals. The heavy traces give the time variations of the angle between the total field vectors, and the thin traces give the variations between the projections of the vectors in the y-z plane. The lag times of the minimum angles between the total and projected fields at the two spacecraft are labeled T_{min-B} and T_{min-yz}, respectively.

The five panels in Figure 2 illustrate five types of variations. In the top two panels the interval of lag time over which the angles are minimal is relatively short and well-defined, especially in the top panel. Plots of this type meet the commonly held expectation that magnetic features observed far upstream are convected downstream with little change, and that their scale size in the outflowing direction is small

relative to the interspacecraft distance. The third panel shows evidence of large-scale wave structure with a period of ~ 30 min and a wavelength of ~ 100 R_E. In cases like this the angle between the fields at the two spacecraft reaches minimal values at several different lag times. In the fourth panel the IMF has essentially the same orientation at the two spacecraft throughout the two-hour period. Thus the scale size of the magnetic feature being observed must be considerably larger than the interspacecraft distance. The fifth panel shows what appears to be a transition from a period like that in the third panel to a time when the fields at the two spacecraft are completely uncorrelated. The lack of correlation may be owing either to temporal changes or to scale sizes perpendicular to the flow direction which are less than the interspacecraft distance in the y-z plane. In the total set of cases, variations of the types shown in panels two, three, and four are about equally common. Only 3% of the cases show the poor correspondence of the fifth panel, and only 6% show the excellent definition of the first pattern.

The vertical lines in Figure 2 mark two predicted lag times. The solid line marks the simple convection lag time $T_{conv} = \Delta x/V$ [e.g., King, 1983], where Δx is the difference in the x coordinates of the two spacecraft positions, and V is the solar wind speed. In using T_{conv} as a predicted lag time, one assumes that surfaces of constant phase in a magnetic feature lie perpendicular to the radial solar wind flow direction. The dashed line marks the lag time based on the IMF orientation, T_{IMF}. It is the same as the corotation lag time [e.g., King, 1983] except that it is calculated from the measured IMF orientation at ISEE 3 rather than the assumed Archimedean spiral orientation.

Figure 3 illustrates how T_{IMF} is determined. The plane of the figure

contains the ISEE 3 position and is parallel to the x-y plane of the geocentric interplanetary medium (GIPM) coordinate system [Bieber and Stone, 1979]. Spacecraft coordinates and magnetic field vectors are transformed from the GSE to GIPM coordinate system by a rotation about their common x axis. The angle of rotation is determined by the requirements that the IMF lie parallel to the $x\text{-}y_{GIPM}$ plane ($B_{Z\text{-}GIPM} \equiv 0$) and that its x and y components have opposite signs. The sign requirement causes the IMF to be directed toward or away from the earth from the "dawn" (+x,-y) quadrant. An IMF vector $\vec{B}$ is drawn through the ISEE 3 position in Figure 3. If it is carried to a projected ISEE 1 position at speed V, then the time it takes to reach that position depends upon the y coordinates of the spacecraft positions as well as the x coordinates. Three different projected ISEE 1 positions are shown, at x distances L_1, L_2, and L_3 from $\vec{B}$. Since $T_{IMF} = L/V$, and $L_1 < L_2 < L_3$, it follows that $T_{IMF\text{-}1} < T_{IMF\text{-}2} < T_{IMF\text{-}3}$. In the case of position 2, the two spacecraft have the same y coordinate, so that $L_2 = \Delta x$, and $T_{IMF\text{-}2} = T_{conv}$. In general the ISEE 1 spacecraft lies either above or below the plane of the figure. Thus in using T_{IMF} as a predicted lag time, one assumes that surfaces of constant phase in a magnetic feature lie perpendicular to the $x\text{-}y_{GIPM}$ plane as well as parallel to $\vec{B}$.

In the top panel of Figure 2, T_{IMF} is nearly identical to T_{conv}. Near coincidence of T_{IMF} and T_{conv} can occur either when the y_{GIPM} distance between the spacecraft is small, as in the center position in Figure 3, or more commonly when the x component of the IMF is small. What is remarkable about the predicted lag times in the top panel is that they also coincide with the lag times of minimum angle, T_{min}. In the second panel the predicted lag times are widely separated: T_{IMF} differs from T_{conv} by 31 min. The former clearly is the better predictor in this case, since it lies

within the well of minimum angle between the two spacecraft IMF orientations In the remaining panels, $T_{IMF} \approx T_{conv}$, as in the top panel, but they do not coincide with the T_{min} values. The predicted lags in the third panel indicate which of the several minimum angle wells in the wave structure corresponds to the same solar wind parcel passing the two spacecraft. Interestingly, it is not the well containing either of the T_{min} values. Although T_{conv} and T_{IMF} are within about 5 min of what appears to be the true lag time at the nearest local minimum, the differences between T_{conv} or T_{IMF} and T_{min} are much larger and contribute unwarranted spread to the statistical distributions of lag time differences shown later. In the fourth and fifth panels the T_{min} values are relatively meaningless. Even though the IMF orientations at the two spacecraft are well-correlated in the fourth panel, the lack of time variation of the angle between them affords no information about lag times. Cases like this also contribute large spread to the time lag difference histograms but sharpen the histograms of angular differences at predicted lag times. The fifth panel has large time variations, but lag time comparisons are not useful here either because of the increasingly poor correlation between the two IMF orientations throughout the interval.

Statistical Distributions of Angular Differences. Figure 4 shows histograms of the angle between the IMF at ISEE 1 and ISEE 3 at no lag time T_o (top panels), at the convection lag time T_{conv} (middle panels), and at the IMF orientation lag time T_{IMF} (bottom panels). The left panels give the angles between the total IMF vectors, and the right panels give the angles between their y-z projections. The angles below which 50% (medians) and 80% of the cases fall are listed in Table 1 along with the mean angle for each histogram.

The gentle peaks on the distributions of angles at T_o indicate that the fields remain somewhat correlated even when no transport time is taken into account. Similar results were found by King [1983]. Half of the cases have angles less than ~ 35°, and 80% less than ~ 65°, both for the total and the projected IMF vectors. However, these statistics are improved considerably at the predicted lag times. At T_{conv}, half of the cases have angles less than 20°, and 80% less than 38°. At T_{IMF}, the angles are reduced only by ~ 1°.

Additional histograms are shown in Figure 5. At the top are the angular distributions at the lag time T_{min}. They give the smallest angular difference between the IMF at the two spacecraft within each two-hour data segment. Thus they represent an upper limit on how well the IMF near the earth can be predicted by using time-lagged measurements from a libration-point-orbiting spacecraft. Half of the cases have angles less than ~ 10°, and 80% less than ~ 15° (see Table 1). A comparison between these histograms for T_{min} and the histograms for T_{conv} in the middle panel, r produced from Figure 4, indicates the degree of uncertainty introduced by using a predicted lag time. The histograms in the bottom panel are a quantitative measure of that uncertainty. They give the distribution of the difference between the minimum angle and the angle at the predicted lag time. (Note that these difference distributions are not the result of a simple subtraction of the above distributions.) Table 1 indicates that the median angles at T_{conv} are ~ 8° larger than the median minimum angles.

In order to test the sensitivity of the angle at T_{conv} to lag time, a histogram of the smallest angle within 5 min of T_{conv} was constructed (not shown). The mean of this distribution is 37°, 6° less than the mean of the

distribution for T_{conv}. This value translates roughly into an average slope of 35° per half hour of lag time for the sides of the wells of minimum angle in the lag time versus angle plots, as in Figure 2.

Figure 6 shows normalized angular distributions of cases selected according to whether the interspacecraft distance D in the y-z plane was less than 55 R_E or greater than 90 R_E. The top, middle, and bottom panels give the angles between the total IMF vectors at the two spacecraft at lag times T_{conv}, T_{IMF}, and T_{min}, respectively. It is clear that the angles are smaller for smaller D, in agreement with Crooker et al. [1982]. The lower half of Table 1 lists the medians, means, and 80% levels of the distributions for the two categories. Overall, the values for small D are ~ 30% better than those for large D, with the most improvement (~ 35%) for the T_{conv} distributions. Table 1 also lists the medians, means, and 80% levels for distributions of the angles in the y-z plane (not shown). The improvement in these values for smaller D is less, ~ 15-20%.

Time Lag Statistics. The average time for a magnetic feature to travel from ISEE 3 to ISEE 1 was ~ 55 min during the period studied. This value was determined from histograms (not shown) of the lag time T_{min}, when the angle between the IMF vectors at the two spacecraft reached its minimum value. The median and modal values of these distributions for both the full and projected vectors are 53 min.

Histograms of the difference beween T_{min} and the predicted lag times T_{conv} and T_{IMF} are shown in Figure 7. They are approximately symmetric about zero and peak there. Thus the predicted lags are neither systematically too long nor too short. The peaks for $T_{min} - T_{IMF}$ rise more sharply than those for $T_{min} - T_{conv}$, indicating that T_{IMF} is a somewhat better prediction. For example, in the total vector histograms on the left, 48% of

the $T_{min} - T_{IMF}$ values lie within ± 10 min of zero, compared to 40% of the $T_{min} - T_{conv}$ values.

These results suggest that IMF features tend to conform to the geometry in Figure 3, for which T_{IMF} was designed. In order to test the strength of this tendency, the $T_{min} - T_{conv}$ histograms in the top half of Figure 7 were separated according to whether L is less than or greater than Δx. If $L < \Delta x$, as is L_1 in Figure 3, then the observed lag time T_{min} should be less than T_{conv}, since the solar wind has a shorter distance to travel to bring the magnetic feature $\vec{B}$ to ISEE 1 than to travel the full x distance between the spacecraft. If $L > \Delta x$, as is L_3 in Figure 3, then T_{min} should be greater than T_{conv}.

The results of this test are shown in Figure 8. In order to reduce the noise level, cases with $|L-\Delta x| < 10R_E$ were eliminated. The top panel is for the total field vector differences, and the bottom for the y-z projections. It is clear in both panels that the distribution of cases with $L < \Delta x$ peaks on the negative side of the $T_{min} - T_{conv}$ axis, and vice versa, in agreement with the prediction.

Discussion and Conclusions

The main conclusion to be drawn from this study is that the IMF orientation near the sunward libration point, lagged simply by the time required for the solar wind to convect to the earth, is a reasonably good predictor of IMF orientation near the earth. Specifically, there is a 50% (80%) probability that a ten-minute averaged predicted IMF vector lies within 20^o (38^o) of its true direction. The probabilities are essentially

the same for the y-z vector projections.

A second conclusion is that a lag time T_{IMF} based on the assumption that magnetic features tend to be aligned with the observed field direction, is clearly more accurate than the simple convection lag time T_{conv}. However, on a statistical basis, the difference in the two predicted lag times is not large enough to improve significantly the distribution of angular differences between the IMF vectors at the two spacecraft. Thus, since T_{conv} is much more convenient to calculate than T_{IMF}, the IMF orientation at T_{conv} remains the predictor of choice.

The uncertainty in the predicted IMF orientation has two components. The first results from uncertainty in the lag time: The angle between the libration point IMF vector and the near-earth vector is always larger at T_{conv} than at T_{min}, unless $T_{conv} = T_{min}$, since by definition T_{min} is the lag time when the angle reaches its minimum. There is a 50% (80%) probability that this angular difference for a ten-minute averaged vector is less than 8^{o} (20^{o}). The second component of uncertainty results from temporal changes in IMF orientation as the solar wind convects from the libration point to the earth, and also from spatial scales of magnetic features which are smaller than the y-z projection of the distance from the earth to the libration-point-orbiting spacecraft. It is these variations which prevent the angle between IMF orientations at the two spacecraft from reaching zero at T_{min}. There is a 50% (80%) probability that a ten-minute averaged IMF vector at the libration point will lie within 11^{o} (19^{o}) of the orientation of a ten-minute averaged vector near the earth during the following two-hour period. Thus the two components of uncertainty are about equal and account for the total uncertainty in the predicted IMF orientation given by the probabilities above.

The final conclusion concerns the improvement in the predicted IMF orientation which may be obtained by restricting the data to those times when the libration point orbit is within some distance D of the earth-sun line. As mentioned in the introduction, Crooker et al. [1982] found that the correlation between fields at ISEE 3 and ISEE 1 falls sharply for D > 90 R_E. The results here indicate that the angles between the fields at the two spacecraft are about 30% smaller for D < 55 R_E than for D > 90 R_E. However, the statistical improvement gained by simply restricting cases to D < 90 R_E is considerably less, about 10%. Specifically, there is a 50% (80%) probability that the predicted IMF vector is within 18° (33°) of its true direction in the restricted data set, compared to within 20° (38°) for the total data set.

Although the subject of scale sizes of magnetic features is covered elsewhere [e.g., Crooker et al., 1982], additional information on scale size along the earth-sun line is obtained from this study. The histograms of angles between the IMF at the two spacecraft for no time lag (top of Figure 4) indicate that features often span the x distance between the spacecraft, ~ 200 R_E. Further, scale sizes greater than 400 R_E along the earth-sun line (x-axis) must have been present about a third of the time during the period studied. Roughly a third of the cases had essentially the same IMF orientation at the two spacecraft over the length of the two-hour data segments analyzed, as in the fourth panel of Figure 2, and the solar wind normally covers a distance of more than 400 R_E during two hours.

The period of time covered by the study was near the maximum phase of the solar cycle, when large scale coronal mass ejections occurred at a rate of ~ 1/day [Hundhausen et al., 1984]. These ejections may account for the large scale sizes deduced from our study. Since the scale size of their

magnetic features is inferred to be ~ 5000 R_E [e.g., Klein and Burlaga, 1982; Crooker, 1983], only about 1/3 of the ejections would be required to pass in the earth's vicinity to account for the frequency of the signatures in the fourth panel of Figure 2.

Acknowledgements. The authors thank J. Farrara (UCLA), K. Y. Yamasaki (UCLA), J. Wolf (JPL), and especially D. G. Sibeck (UCLA) and J. A. Slavin (JPL) for their willing assistance. This work was supported by the National Aeronautics and Space Administration under grants NSG 5351 (UCLA), NAS5-28448 (UCLA), and NAS7-100 (JPL), and under subcontract 955376 (JPL to UCLA).

References

Beiber, J. W., and E. C. Stone, Energetic electron bursts in the magnetopause electron layer and in interplanetary space, in Magnetospheric Boundary Layers, edited by B. Battrick, pp. 131-135, ESA SP-148, Paris, 1979.

Burch, J. L., Energy transfer in the quiet and disturbed magnetosphere, Rev. Geophys. Space Phys., 21, 463-473. 1983.

Crooker, N. U., G. L. Siscoe, C. T. Russell, and E. J. Smith, Factors controlling degree of correlation between ISEE 1 and ISEE 3 interplanetary magnetic field measurements, J. Geophys. Res., 87, 2224-2230, 1982.

Crooker, N. U., Solar cycle variations of the solar wind, in Solar Wind Five, edited by M. Neugebauer, NASA CP-2280, pp. 303-313, 1983.

Hundhausen, A. J., C. B. Sawyer, L. House, R. M. E. Illing, and W. J. Wagner, Coronal mass ejections observed during the solar maximum mission: Latitude distribution and rate of occurrence, J. Geophys. Res., 89, 2639-2646, 1984.

King, J. H., Interplanetary Medium Data Book, Supplement 2, 1978 - 1982, Rept. NSSDC 83-01, Goddard Space Flight Center, Greenbelt, Maryland, 1983.

Klein, L. W., and L. F. Burlaga, Interplanetary magnetic clouds at 1 AU, J. Geophys. Res., 87, 613-624, 1982.

Russell, C. T., G. L. Siscoe, and E. J. Smith, Comparison of ISEE 1 and 3 interplanetary magnetic field observations, Geophys. Res. Lett., 7, 381-384, 1980.

TABLE 1. Characteristics of Distributions of Angular Differences Between IMF Vectors at ISEE 1 and ISEE 3

Lag Time	Total Vector / y-z Projection Mean	Median	80% Level
	ALL CASES (885)		
T_o	36°/34°	43°/46°	63°/69°
T_{conv}	20°/18°	26°/27°	38°/38°
T_{IMF}	19°/16°	25°/25°	37°/37°
T_{min}	11°/6°	13°/10°	19°/14°
$T_{conv} - T_{min}$	8°/9°	13°/15°	29°/25°
$T_{IMF} - T_{min}$	7°/8°	12°/15°	18°/22°
	CASES WITH D < 55 R_E (414)		
T_{conv}	17°/15°	22°/24°	31°/34°
T_{IMF}	16°/14°	22°/22°	30°/32°
T_{min}	9°/7°	11°/10°	17°/14°
	CASES WITH D > 90 R_E (221)		
T_{conv}	26°/20°	32°/31°	49°/48°
T_{IMF}	23°/17°	29°/28°	45°/40°
T_{min}	13°/8°	15°/11°	21°/16°

List of Figures

Fig. 1. ISEE 3 orbit in GSE coordinates from July 25 to Nov. 27, 1979. The shaded region in the upper panel indicates the simultaneous coverage of ISEE 1.

Fig. 2. Examples of variations in the angle between the IMF at ISEE 1 and ISEE 3 as a function of lag time. The solid traces give the angle between the total vectors, and the dash-dot traces between the projections of the fields in the y-z plane. The vertical solid and dashed lines mark the predicted lag times T_{conv} and T_{IMF}, respectively. Arrows labeled T_{min} mark the lag times of minimum angle between the total vectors (B) and between the y-z projections (yz).

Fig. 3. Schematic diagram illustrating the geometry for calculating T_{IMF}. The plane of the diagram is parallel to the $x\text{-}y_{GIPM}$ plane and contains the ISEE 3 position, through which an IMF vector $\vec{B}$ is drawn. Three possible projected ISEE 1 positions 1, 2, and 3 are shown (not to scale). The vector $\vec{B}$ convects to positions 1, 2, and 3 over distances L_1, L_2, and L_3 at the solar wind speed V. Since $L_1 < L_2 < L_3$, the transit time T_{IMF} is shortest for position 1 and longest for position 3. At position 2, $T_{IMF} = \Delta x/V = T_{conv}$, where Δx is the difference in x coordinates of the ISEE 1 and ISEE 3 positions.

Fig. 4. Histograms of the angle between the IMF at ISEE 1 and ISEE 3 at zero lag time T_o and at the predicted lag times T_{conv} and T_{IMF}. Angles between the total vectors B are on the left, and angles between their y-z projections are on the right.

Fig. 5. Histograms of the angle between the IMF B vectors and y-z projections at ISEE 1 and ISEE 3 at T_{conv}, from Figure 4, and at T_{min}, the lag time when the angle reaches its minimum in each two-hour data segment. In the bottom row are histograms of the difference between the angle at T_{conv} and the minimum angle, at T_{min}.

Fig. 6. Comparison of histograms of the angle between the IMF B vectors at ISEE 1 and ISEE 3 at T_{conv}, T_{IMF}, and T_{min} for $D < 55\ R_E$ (414 cases) and $D > 90\ R_E$ (221 cases), where D is the interspacecraft distance in the y-z plane. The histograms are normalized to percentages to facilitate comparison.

Fig. 7. Histograms of the differences between the lag time at minimum angle T_{min} and the predicted lag times T_{conv} and T_{IMF} for the IMF B vectors and y-z projections.

Fig. 8. Comparison of histograms of $T_{min} - T_{conv}$ for $L < \Delta x$ (405 cases) and $L > \Delta x$ (194 cases). These conditions are illustrated at positions 1 and 3, respectively, in Figure 3. Cases with $|L - \Delta x| < 10\ R_E$ were eliminated to reduce noise. As predicted, cases with $L < \Delta x$ have shorter lag times T_{min} than the predicted lag times T_{conv}, and vice versa.

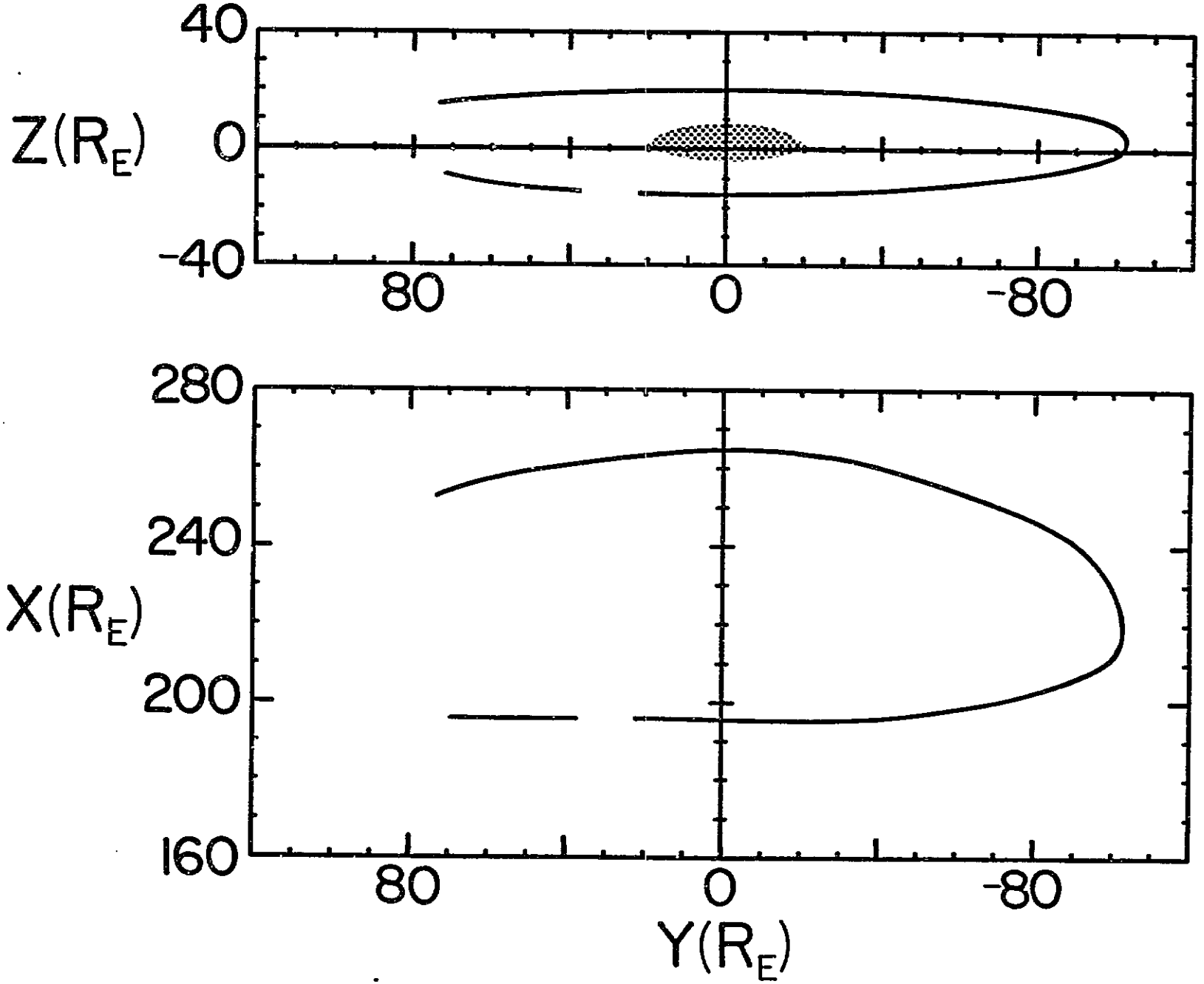
40
0
-40
Z(R_E)
80
0
-80
280
240
200
160
X(R_E)
80
0
-80
Y(R_E)

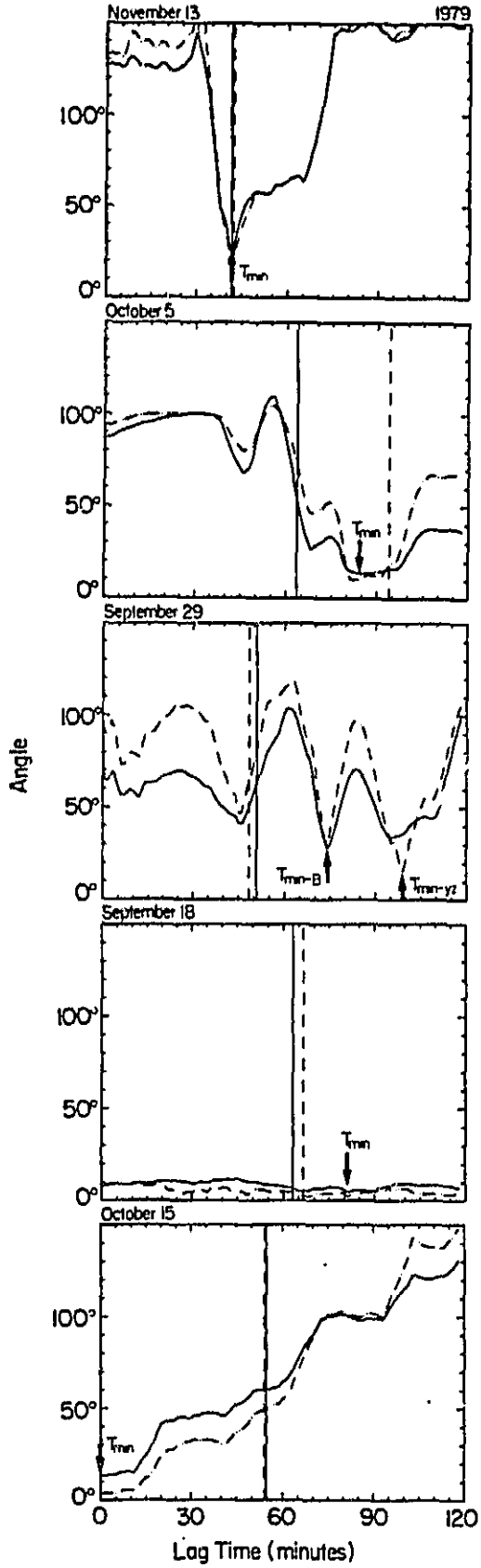
November 13
1979
October 5
September 29
September 18
October 15
100°
50°
0°
Angle
T_{min}
T_{min-B}
T_{min-yz}
0
30
60
90
120
Lag Time (minutes)

Figure 2

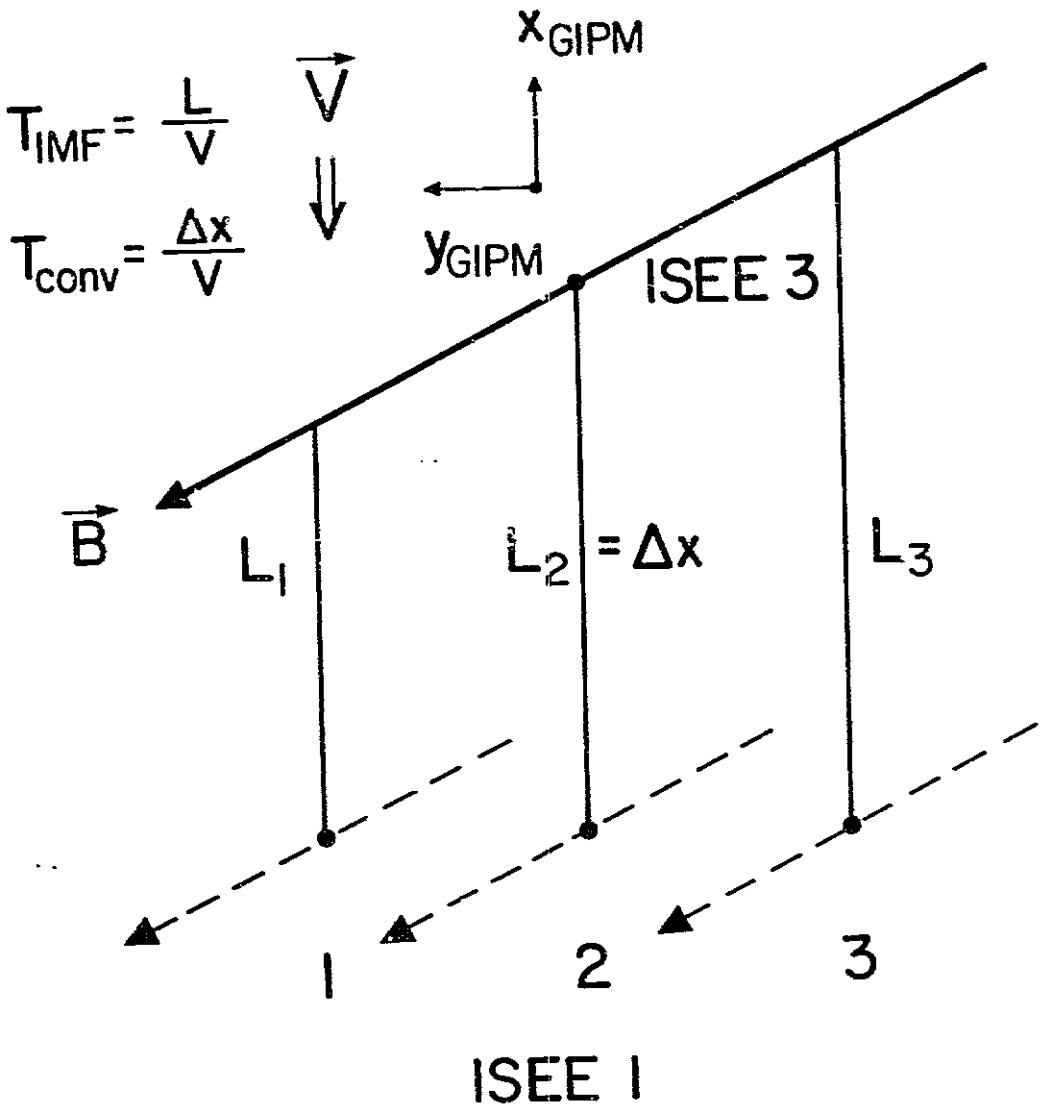
$T_{IMF} = \frac{L}{V}$
$T_{conv} = \frac{\Delta x}{V}$
$\vec{V}$
x_{GIPM}
y_{GIPM}
ISEE 3
$\vec{B}$
L_1
$L_2 = \Delta x$
L_3
1
2
3
ISEE 1

Figure 3

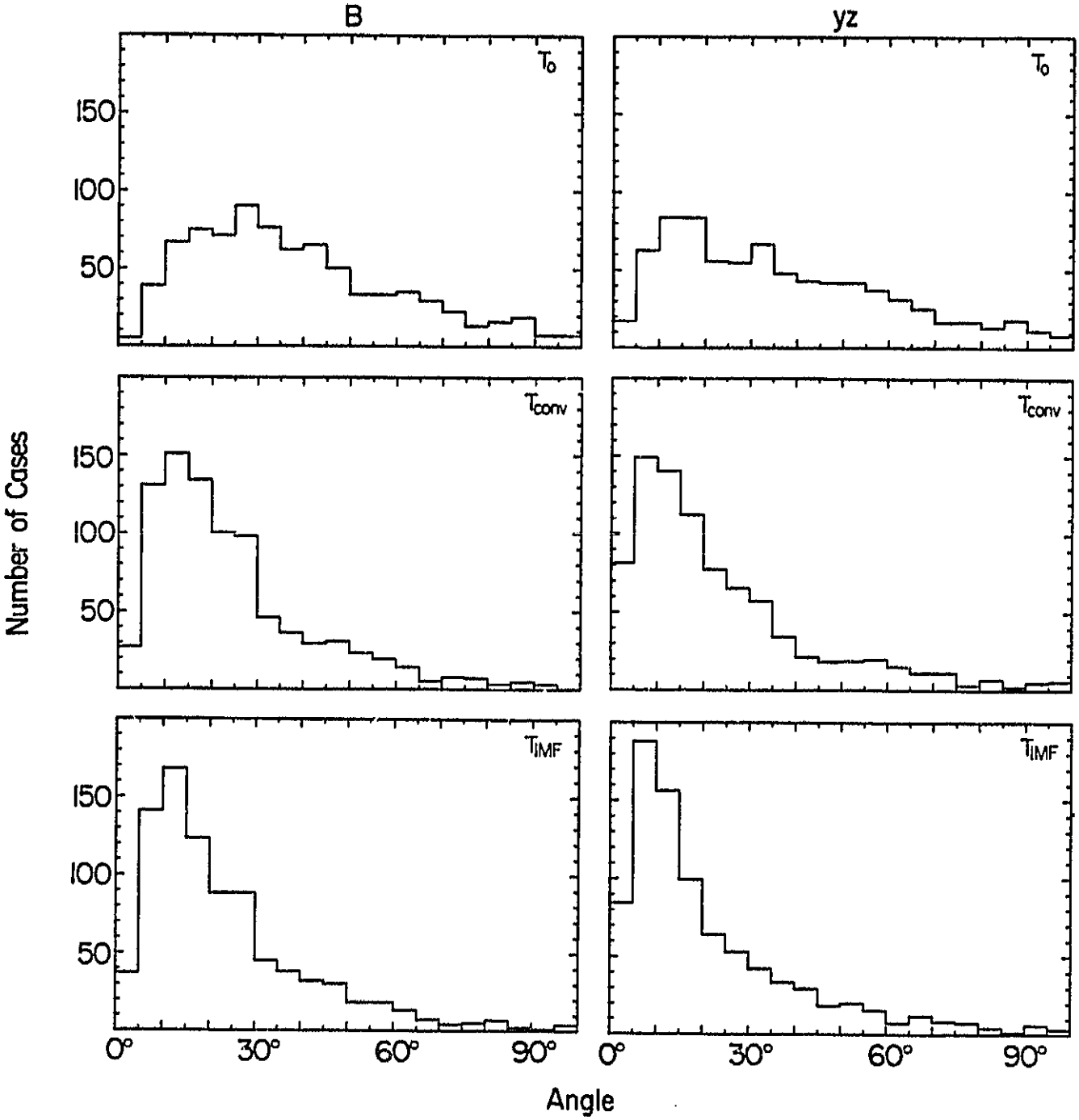

Figure 4

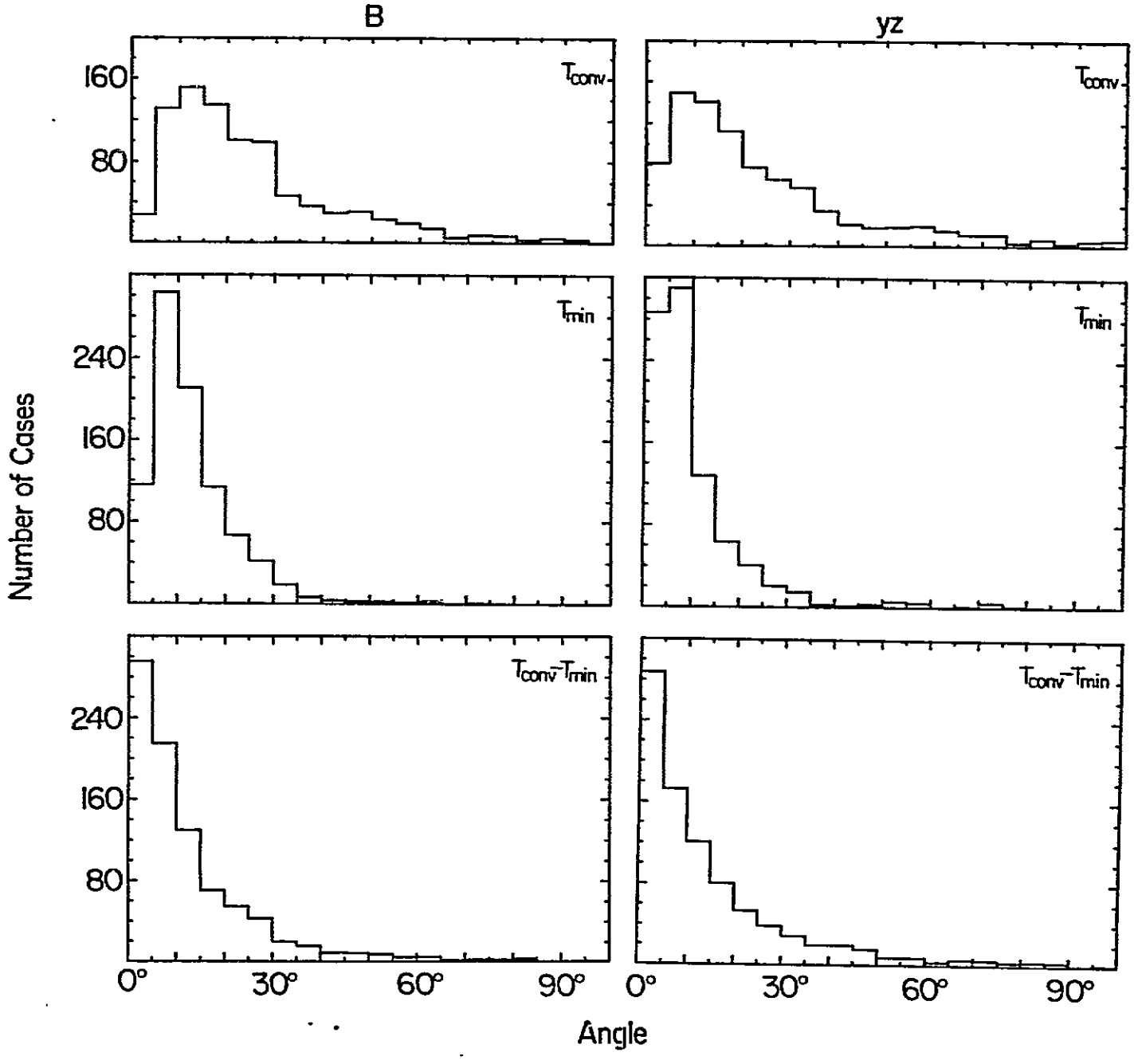
B
yz
T_{conv}
T_{min}
$T_{conv}-T_{min}$
160
80
240
160
80
240
160
80
Number of Cases
0°
30°
60°
90°
0°
30°
60°
90°
Angle

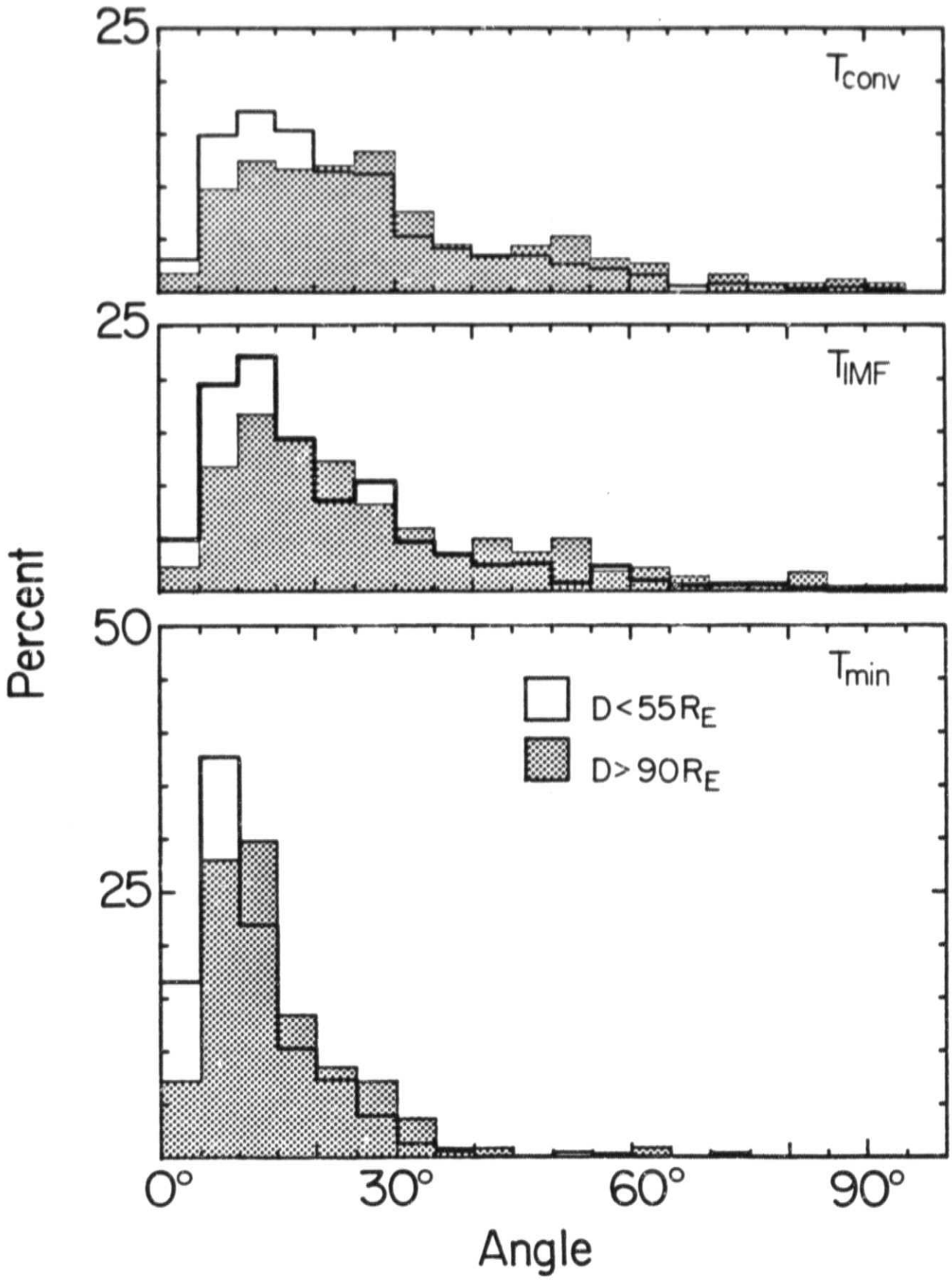
25
T_{conv}
25
T_{IMF}
50
T_{min}
$D<55R_E$
$D>90R_E$
25
Percent
0°
30°
60°
90°
Angle

Figure 6

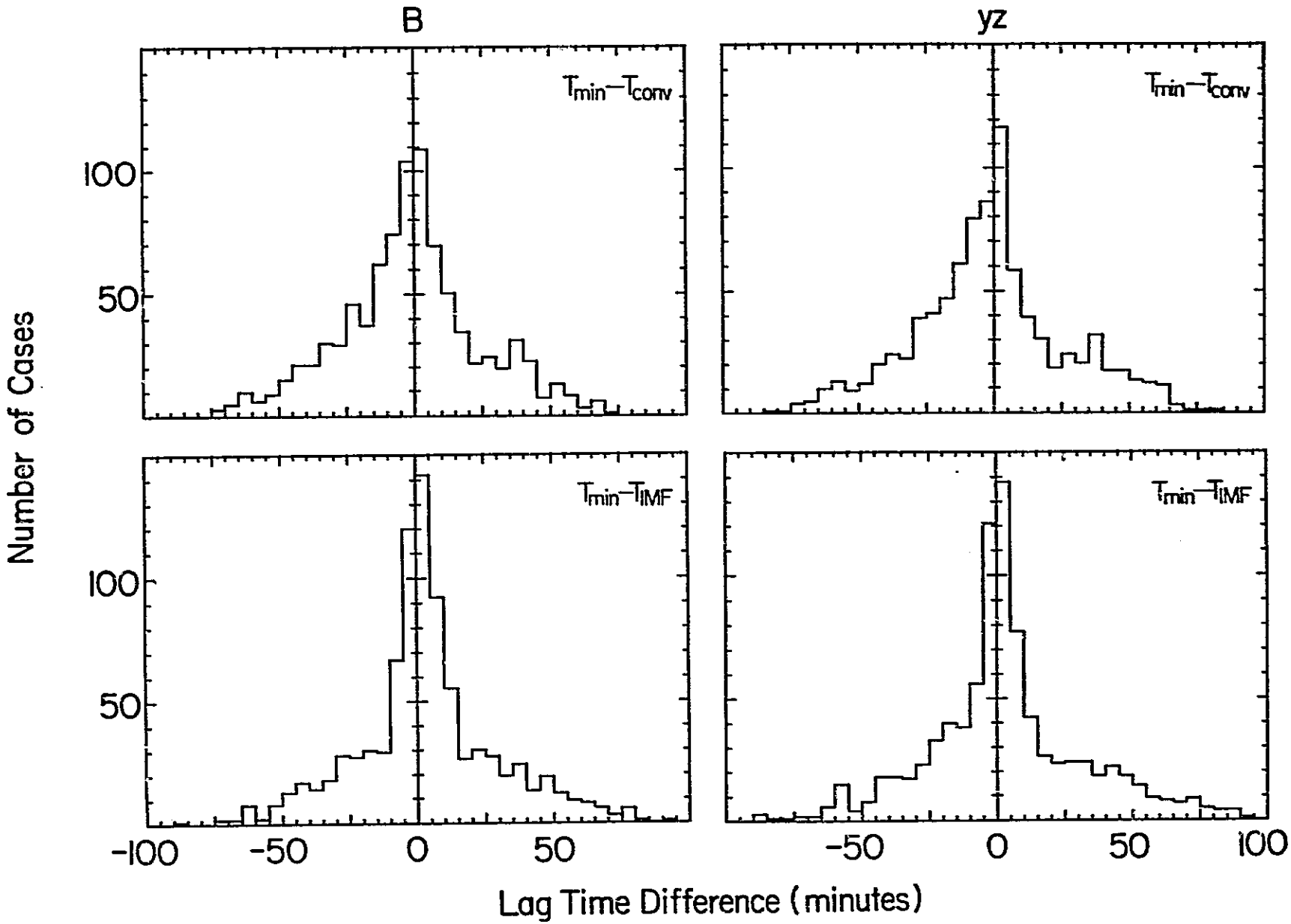
B
yz
$T_{min}-T_{conv}$
$T_{min}-T_{IMF}$
Number of Cases
100
50
-100
-50
0
50
100
Lag Time Difference (minutes)

Figure 7

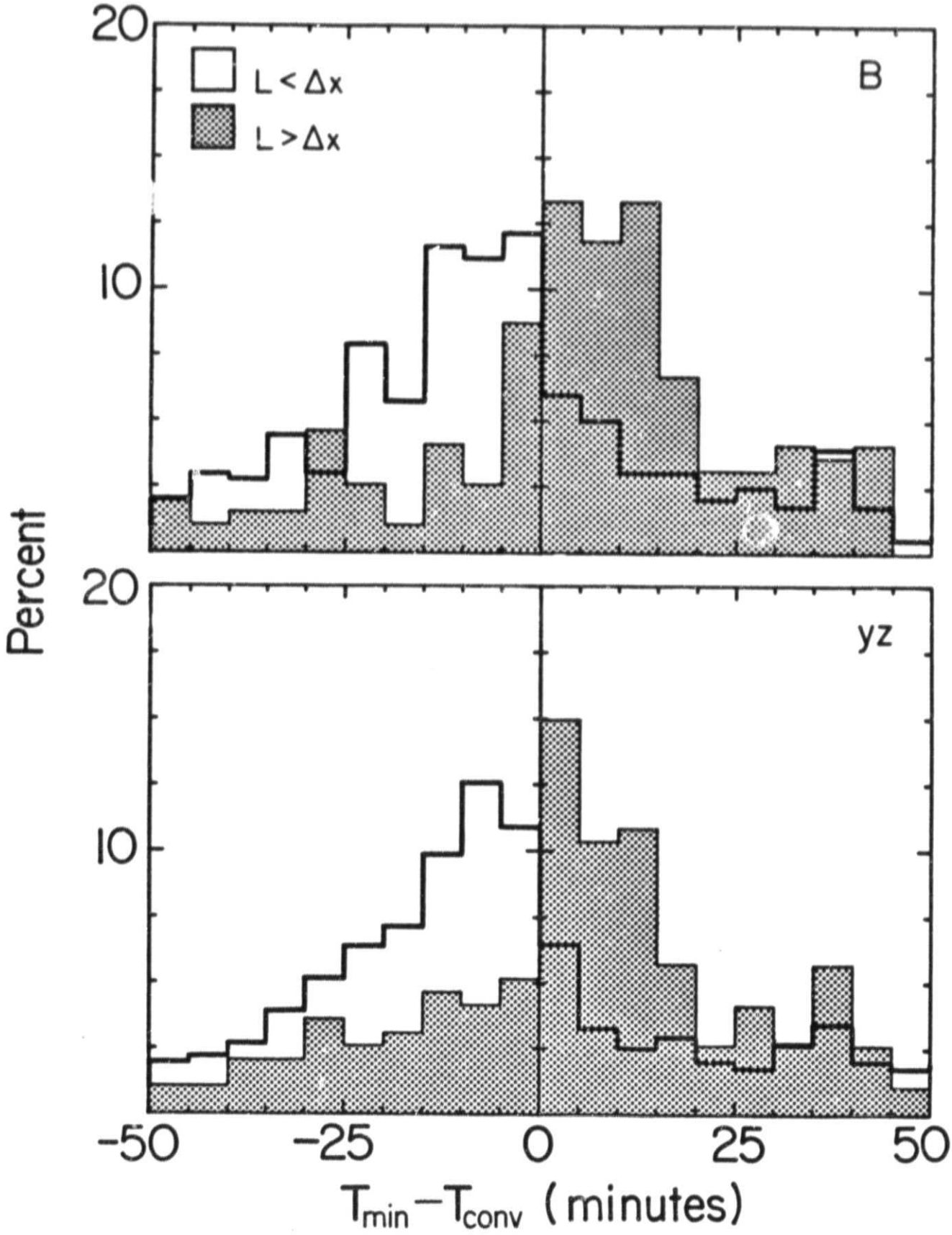

Figure 8